Biodesign

pISSN 2288-6982 | eISSN 2288-7105

TECHNICAL REPORT P 12-23

Structure determination of the C-terminal fragment of yeast Ski7 using twinned crystal data

Si Hoon Park[1,+], Yong-Boo Kuk[1,+], Ji-Young Lee[1], Byeong-Cheon Jeong[1] and Hyun Kyu Song[1,2,*]

[1]Department of Life Sciences, Korea University, 145 Anam-ro, Seongbuk-gu, Seoul 02841, Korea, [2]Center for Molecular Dynamics and Spectroscopy, Institute of Basic Science, Seoul 02841, Korea. *Correspondence: hksong@korea.ac.kr

[+]These authors contributed equally to the work.

The structure determination using twinned crystals is challenging although several algorithms have been developed for detwinning the X-ray data. Our crystal of the C-terminal domain 2 and 3 of Ski7 (Ski7-D2/3), a key part of non-stop mRNA decay has a perfect twin with the twin operator [h, -h-k, -l]. Many different efforts for phasing with multiple anomalous dispersion techniques using selenomethionine substituted wild-type and mutant proteins were not successful and the phases were obtained through the molecular replacement method using recently reported structure of C-terminal GTPase domain of Ski7 from *Saccharomyces cerevisiae.* The overall structure of Ski7-D2/3 is very similar to that of the corresponding domain of ribosome-associated GTPases including eIF5B, eEF1α, and eRF3. Domains 2 and 3 form a β-barrel structure containing several structurally deviated long connecting loops. Although the linker between domain 2 and 3 is very flexible, the relative orientation between them is virtually the same among all structures, showing that the Ski7-D2/3 does not show major conformational movement upon contacting with G domain.

INTRODUCTION

Surveillance mechanisms detect and degrade aberrant mRNAs for ensuring fidelity and quality of mRNA in the cells. There are three pathways of mRNA surveillance; nonsense-mediated decay (NMD), no-go decay (NGD), and non-stop decay (NSD) (Doma & Parker, 2007). NMD detects transcripts containing premature stop codons (PTCs). When a ribosome terminates its translation in the PTC, the NMD factors, Upf and Smg associate and target the mRNA for degradation (Garneau et al., 2007; Lykke-Andersen & Bennett, 2014). NGD detects and degrades transcripts that block translation by stable RNA hairpin structures. The evolutionary conserved Hbs1 and Dom34 complex plays a critical role in NGD (Lykke-Andersen & Bennett, 2014; Shoemaker et al., 2010; Matsuda et al., 2014; Lee et al., 2007). NSD is involved in the detection and decay of mRNA transcripts which lack a stop codon (Matsuda et al., 2014; Inada, 2013). A ribosome translating the mRNA eventually encounters and stalls at the 3'poly-A tail region of transcripts without a stop codon. It is a crucial problem for the cells because the ribosome cannot eject the mRNA.

For NSD, Ski7 (superkiller protein 7) specifically recognizes this stalled ribosome and recruits Ski complex (Ski2/Ski3/Ski8) and exosome for RNA degradation in *Saccharomyces cerevisiae*. Previous biochemical studies show that Ski7 interacts with the stalled ribosome by C-terminal domain, and recruits cytoplasmic exosome and Ski complex (Ski2/3/8) by N-terminal domain (van Hoof et al., 2002; Frischmeyer et al., 2002; Halbach et al., 2013; Kowalinski et al., 2015; Schaeffer et al., 2009; Lee et al., 2014). The Ski7 belongs to a family of ribosome-associated GTPases, which comprise essential translational factors such as eIF5B, eEF1α, and eRF3. All ribosome-associated GTPases carry a highly conserved GTPase domain, adjacent to β-barrel domains (Atkinson, 2015). The Ski7 shares the structural similarity with the ribosome-associated GTPase domains and tmRNA (transfer-messenger RNA) that interacts with ribosomal A site in prokaryotic NSD pathway and might interact with ribosomal A site (van Hoof et al., 2002; Karzai et al., 2000; Gutmann et al., 2003). Interestingly, the NSD also exists in mammals, but there is no Ski7 homolog and thus it has been suggested that Hbs1 and Dom34 complex participates in the NSD pathway in mammalian cells (Tsuboi et al., 2012; Saito et al., 2013).

The ribosome-associated GTPases form a heterodimer with a binding partner such as Hbs1 for Dom34 and eRF3 for eRF1, but the binding partner of Ski7 has not yet identified (Shoemaker & Green, 2012; Kowalinski et al., 2015). The GTPase activity is crucial for the specificity of eEF1α, eRF3, Hbs1, EF-Tu and needs a conserved histidine residue at the active site (Daviter et al., 2003). However, Ski7 has no conserved histidine residue. Therefore, Ski7 may achieve its function without hydrolyzing GTP and indeed, it has a very limited GTPase activity (data not shown) and very recently, Kowalinski et al. also reported that Ski7 has unique features in the GTP-binding site and may have enhanced GTP-binding properties, but not GTP-hydrolysis (Kowalinski et al., 2015). All ribosome-associated GTPases possess GTP-binding G domain and additional β-barrel domains,

domain 2 and 3. The domain 2 and 3 (hereafter, D2/3) contact with G domain, and its relative orientation to the G domain is important for regulating the function of ribosome-associated GTPases. Although the structure of the D2/3 of Ski7 (Ski7-D2/3) is predicted to be similar to that of the other D2/3 domains (Chen, Muhlrad, et al., 2010; Kong et al., 2004), the primary sequence of Ski7-D2/3 has a very limited sequence similarity to that of eRF3 and Hbs1 (Lee et al., 2014), and thus, there might be unique features.

Previously, we reported a preliminary crystallographic data of Ski7-D2/3 crystals (Lee et al., 2014) and conventional multiple anomalous dispersion (MAD) approach has been applied for phase determination. However, we have identified the serious twinning problem of our crystals. Many different efforts have been tried for obtaining phases with these twinned crystals, but unfortunately, the crystal structure of the C-terminal region of Ski7 has been published very recently (Kowalinski et al., 2015). Although the structure of Ski7-D2/3 has been finally determined by molecular replacement (MR) method, our attempts at overcoming the twinning problem will be described in this paper.

RESULTS AND DISCUSSION

X-ray data analysis of Ski7-D2/3 crystal

Our initial construct, whole C-terminal domain of Ski7 (residues 254-747) was soluble using His6-RIP tag (Lee et al., 2012) whereas full length Ski7 with GST-tag was not soluble in *E. coli*. However, the crystallization of the C-terminal domain of Ski7 alone and its complex with GMP-PNP or GDP was not successful. Fortunately, the smaller fragment, Ski7-D2/3 (residues 520–747) was crystallized, as described previously (Lee et al., 2014). The crystal diffracted to 2.0 Å resolution and the X-ray data has been collected, and thus, we initially thought that the structure determination might be straightforward. As a first step, MR has been tried, using the similar structural domain in Hbs1 (Chen, Muhlrad, et al., 2010). The solution, however, was not clear, suggesting that the structure of Ski7-D2/3 might be significantly different from that of Hbs1 domain 2 and 3. The expression level of selenomethionine (SeMet) substituted Ski7-2/3 fused with GST was much lower than native protein and thus we have changed the expression vectors (See METHODS for details). The SeMet crystals were obtained without much difficulty. The 2.87 Å-resolution MAD data has been collected, but the position of Se was not easily found. Initially we thought the number of Se might be a problem for phasing, because there is only one methionine (Met 581) out of 228-residue long Ski7-D2/3 construct (Figure 1). In the meantime, the twinning problem of the crystals was also detected (Figure 2). The crystals belong to a trigonal space group and it is a hemihedral twinning. Twinning in the trigonal space group was reported in several cases (Dauter, 2003) including plastocyanin (Redinbo & Yeates, 1993), hydroxylamine oxidoreductase (Igarashi et al., 1997), bacteriorhodopsin (Luecke et al., 1998), α-lactalbumin (Chandra et al., 1998), N-terminal half of lactoferrin (Breyer et al., 1999), flavodoxin (Guelker et al., 2009), and Δ1-62NtNBCe1-A (Gill et al., 2013). It was not only recognized in diffraction pattern, and previously we reported the crystal belongs to the space group, either P3121 or P3221, which turned out to be the wrong assignment (Figure 3). The twin fraction α of our native crystals is in the range between 0.458 and 0.488 in H-test with the twin operator [h,-h-k,-l] (Table 1).

Approaches for overcoming the twin problem

It has been known that the structure determination with twinned data is not easy and the best way is to obtain new crystal forms or crystals with low twin fraction. We have obtained many crystals of Ski7-D2/3 using different crystallization conditions and also in the presence of diverse additives, but they are basically the same twinned crystals. Therefore, we decided to introduce mutations in the protein and simultaneously tried to increase the number of methionine residues for improving the phase information, which might induce different crystal packing and/or more Se positions for phasing. To introduce methionine residues in Ski7-D2/3, we analyzed the sequence homology using BLAST. Ski7 is a highly conserved and yeast-specific protein, and thus, variable hydrophobic residues were not easily detected. Ski7p from *Saccharomyces arboricola* H-6 (GI: 748454621), Ski7p from *Saccharomyces cerevisiae x Saccharomyces kudriavzevii* VIN7 (GI: 365758398), and Ski7-like proteins from *Saccharomyces kudriavzevii* IFO1802 (GI: 401838887) were aligned with Ski7-D2/3. Four possible mutation sites, Leu588, Ile630, Leu650, and Ile655 were found (Figure 1). We have cloned two mutants, L588M and double L650M/I655M, and purified SeMet-substituted protein for crystallization. SeMet crystals using L588M and L650M/I655M mutants were grown at the same condition with native crystals. However, the L650M/I655M mutant crystal was a little unstable and the diffraction was limited to maximum 3.0 Å resolution. The radiation damage was also severe and thus, we have collected the data with the larger oscillation angle (3 degrees) to reduce radiation damage. In total, 16 different X-ray data sets were collected including several MAD data sets (Table 1). Although more anomalous scatters were included, the phase calculations were not successful. Therefore, the twinning problem is the biggest obstacle for the structure determination of Ski7-D2/3.

Investigation for the twinned data sets

For acentric reflections, the intensity ratio $\langle I^2 \rangle / \langle I \rangle^2$ is 1.5 and 2.0 for perfectly twinned and untwinned, respectively (Yeates & Fam, 1999). Our native crystals show the average intensity ratio is 1.6~1.9 and it highly depends on the resolution of the data. The calculated $\langle I^2 \rangle / \langle I \rangle^2$ ratio using high resolution 2.0 Å data is 1.6, whereas a 2.8 Å resolution data is 1.96 (Table 1). The data sets with SeMet wild-type and L588M mutant crystals show that the $\langle I^2 \rangle / \langle I \rangle^2$ ratio is also around 1.7, however, the SeMet L650M/I655M double mutant crystal shows an almost

untwinned ratio, above 2.0 (Table 1). The other indicators, the Wilson ratio $\langle F \rangle^2/\langle F^2 \rangle$ as well as the intensity statistics $\langle |E^2-1| \rangle$ also show the same trends. For acentric reflections, the Wilson ratio $\langle F \rangle^2/\langle F^2 \rangle$ is 0.885 for perfectly twinned and 0.785 for untwinned, and the $\langle |E^2-1| \rangle$ is 0.541 and 0.736 for perfectly twinned and untwinned, respectively. In general, the values using native and SeMet L588M mutant crystals are closer to the perfect twin whereas those using SeMet L650M/I655M double mutant crystals are somewhat close to the untwinned (Table 1).

Another indicator for twin detection is the local intensity statistic L-test (Padilla & Yeates, 2003). For acentric reflections, the mean |L| value is 0.375 and 0.5 for perfectly twinned and untwinned, respectively and the $\langle L^2 \rangle$ value is 0.200 for twinned and 0.333 for untwinned. The multivariate Z-score L-test value is over and less than 3.5 for perfectly twinned and untwinned, respectively. As shown in Table 1, the L-tests also show similar trends in intensity statics including the Wilson ratio. However, some indicators suggested that SeMet data using L650M/I655M double mutant crystals gave somewhat untwinned or less twinned values and therefore, we have dedicated much effort to MAD phasing of these data sets. However, a better twin law test for each different twin operator gives the same conclusion (Yeates & Fam, 1999). There are 3 possible twin operators because the Ski7-D2/3 crystal belongs to trigonal space group. The hemihedral twinning has twin fraction α between 0.5 for perfect twin and 0.0 for untwinned. If the fraction α is not close to 0.5, the crystal possesses a partial twin and then, detwinning or normal structure determination can be performed. As shown in Table 1, all twin law tests such as the Britton analysis, H-test, and maximum-likelihood method show the different twin fraction α for three, twin operators [-h,-k,l], [h,-h-k,-l], and [-k,-h,-l]. The twin fraction of native and SeMet using L588M mutant crystal is approximately 0.1 for [-h,-k,l] and [-k,-h,-l] operator, but it becomes nearly untwinned with SeMet data using L650M/I655M double mutant crystals. Unfortunately, for the other twin operator [h,-h-k,-l], the twin fraction remains the same, suggesting that it

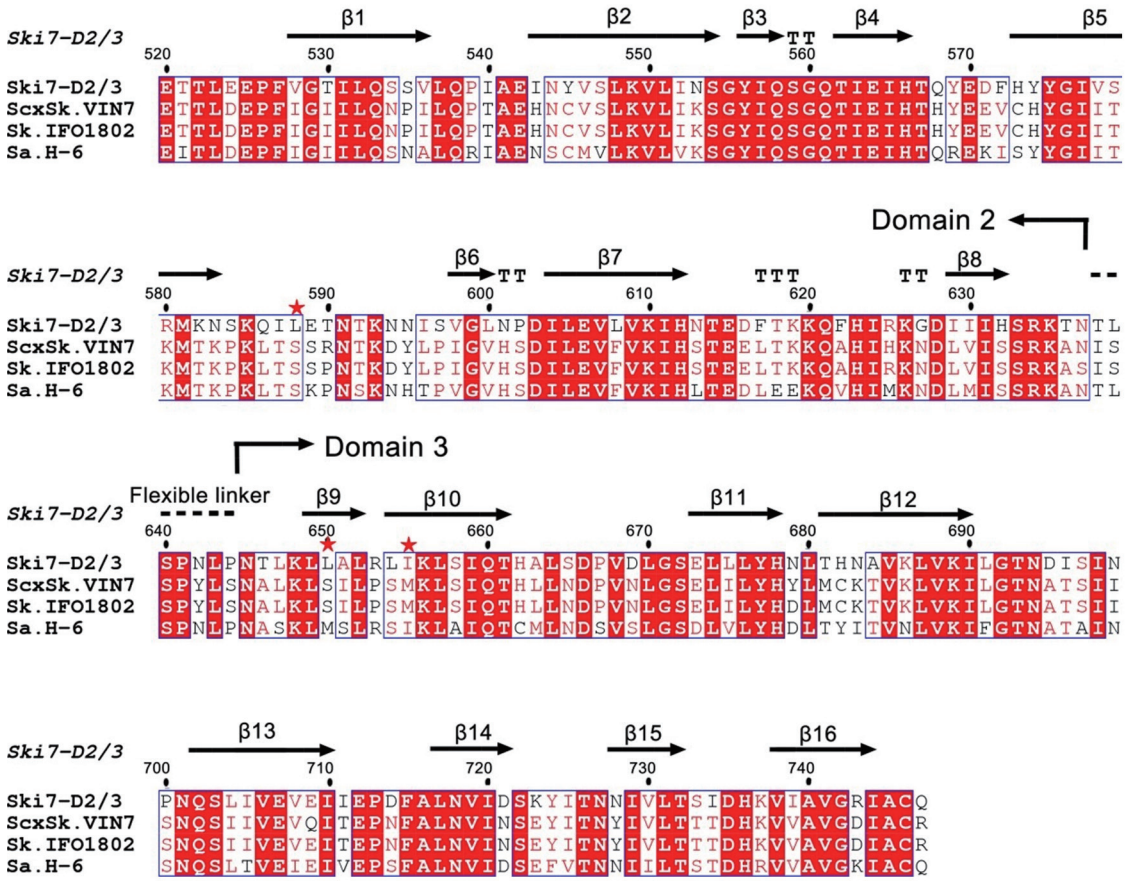

FIGURE 1 | Sequence alignment of domain 2 and 3 of Ski7 from yeast species. Sequence alignment of Ski7-D2/3 orthologs. The following organisms were used: *Saccharomyces cerevisiae* Ski7-D2/3, *Saccharomyces cerevisiae x Saccharomyces kudriavzevii* VIN7, and *Saccharomyces kudriavzevii* IFO1802, and *Saccharomyces arboricola* H-6. The boundary between domains 2 and 3 adopts a flexible linker, which is indicated as black dash. Red shading indicates residues that are identical in all sequences. Secondary structural elements are shown above the sequence alignment. The mutated residues are marked with red stars. Every 10th residue is also indicated above sequence.

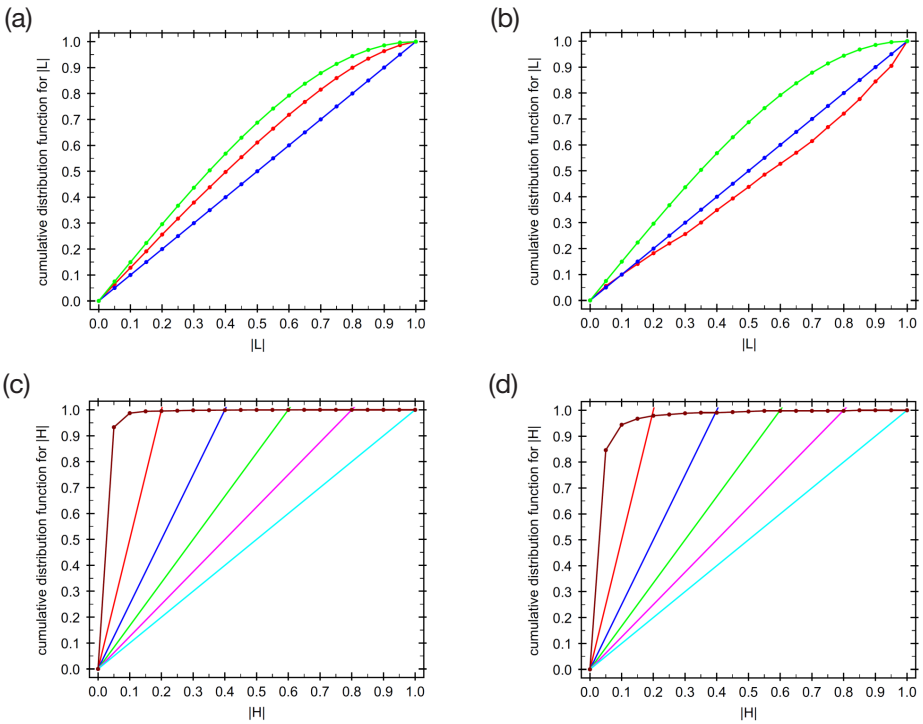

FIGURE 2 | Twinning validation. Cumulative distribution functions for |L| test for (a) native data set and (b) SeMet L650M/I655M data set. Red line represents observed, and blue and green lines represent expected untwinned and twinned, respectively. Cumulative distribution functions for |H| test for (c) native data set and (d) SeMet L650M/I655M data set. The brown line represents the observed twin fraction. Red, blue, green, magenta, and cyan lines are calculated with the twin fraction of 0.4, 0.3, 0.2, 0.1, and 0.0, respectively. The twin fraction α with twin operator [h,-h-k,-l] is 0.47 and 0.44 for native and SeMet double mutant data set, respectively.

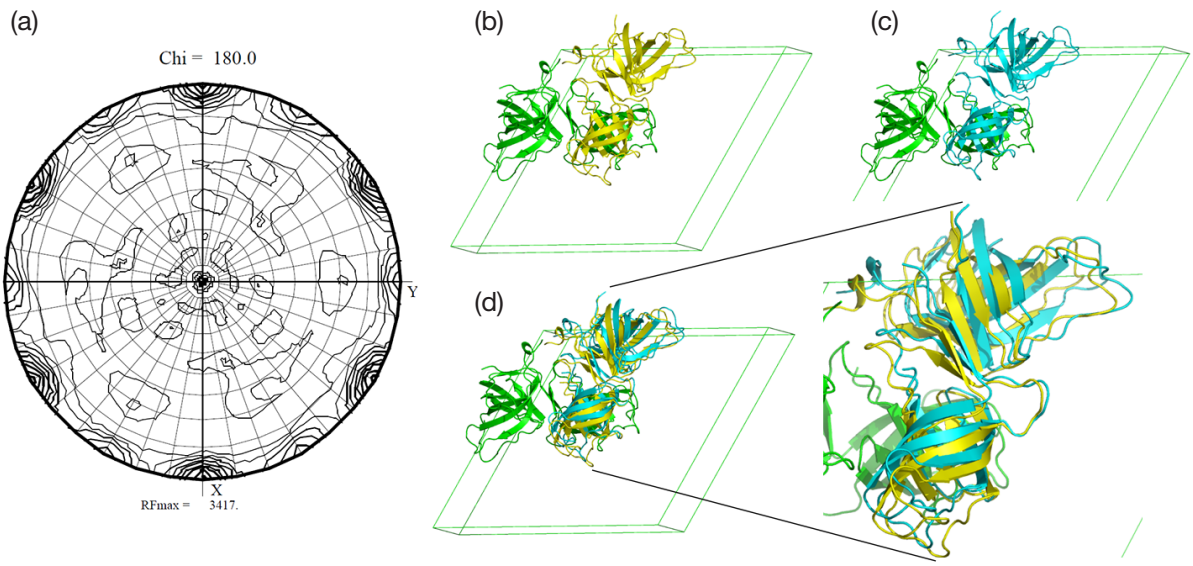

FIGURE 3 | Space group determination. (a) κ=180 section of the self-rotation function of Ski7-D2/3 data. The three-fold symmetry axis in the plan of the paper and a pseudo 2-fold axis perpendicular to the paper are shown. (b) Two molecules of Ski7-D2/3 (green and yellow) were found in the asymmetric unit using the data processed with space group $P3_1$. (c) One molecule of Ski7-D2/3 (green) was found using the data processed with space group $P3_121$. The crystallographic symmetry operation (y, x, -z) generates the second molecule (blue). (d) Superposition of the solutions (green) from two different space groups, $P3_1$ and $P3_121$, and the orientation and position of symmetry equivalent molecule (cyan) in the $P3_121$ packing shows a slight deviation from those of the solution in the $P3_1$ packing (yellow).

TABLE 1 | Experimental data of ski7-D2/3 crystal and twinning test

Data set #	Construct	Space group Resolution range Wavelength	Unit cell parameter a=b/ c	Completeness I/σ(I)	R-symm Rmeas Redundancy	Wilson ratio <F>^{2}/<F^2> I^2/<I>^{2} <|E^2-1|>	L-test Mean |L| Mean L^2 Z-score	Twin law test Twin operator	Britton analysis	H-test	Maximum likelihood method
1	Native [520-747]	P3 50-2.00 (2.03-2.0 0)[a] 0.97933	73.528/ 83.634	99.8 (99.9)[a] 33.8 (1.00)	0.059 (0.820)[a] 0.065 (0.898) 6.3 (6.0)	0.865 1.631 0.579	0.397 0.223 9.873	-h, -k, l h, -h-k, -l -k, -h, -l	0.103 0.454 0.103	0.109 0.486 0.110	0.022 0.478 0.022
2	Native [520-747]	P3 50.0-2.80 (2.85-2.80) 1.25475	73.528/ 83.634	98.7 (100.0) 29.7 (1.44)	0.852 1.740 0.608	0.816 1.960 0.682	0.446 0.275 3.779	-h, -k, l h, -h-k, -l -k, -h, -l	0.039 0.455 0.038	0.068 0.479 0.068	0.022 0.478 0.022
3	Native [520-747]	P3 50.0-2.80 (2.85-2.80) 1.25476	73.758/ 83.716	99.1 (100.0) 52.5 (2.94)	0.077 (0.786) 0.081 (0.819) 12.6 (12.7)	0.824 1.916 0.665	0.446 0.275 3.779	-h, -k, l h, -h-k, -l -k, -h, -l	0.041 0.456 0.041	0.079 0.488 0.078	0.022 0.478 0.022
4	Native [520-747]	P3 50.0-2.00 (2.03-2.00) 0.97950	73.896/ 83.676	99.8 (100.0) 29.4 (2.04)	0.073 (0.889) 0.080 (0.977) 6.3 (6.2)	0.862 1.637 0.581	0.398 0.225 9.678	-h, -k, l h, -h-k, -l -k, -h, -l	0.105 0.454 0.105	0.110 0.488 0.115	0.022 0.478 0.022
5	Native [520-747]	P3 50.0-1.97 (2.00-1.97) 0.97951	73.446/ 83.601	99.3 (100.0) 27.2 (1.33)	0.063 (0.795) 0.074 (0.920) 4.0 (4.0)	0.861 1.656 0.587	0.394 0.221 10.383	-h, -k, l h, -h-k, -l -k, -h, -l	0.103 0.454 0.103	0.106 0.477 0.105	0.022 0.478 0.022
6	Native [520-747]	P3 50.0-2.30 (2.34-2.30) 0.97951	73.420/ 83.869	99.8 (100.0) 23.8 (1.31)	0.097 (0.759) 0.107 (0.828) 6.1 (6.3)	0.852 1.740 0.608	0.410 0.236 7.689	-h, -k, l h, -h-k, -l -k, -h, -l	0.092 0.451 0.086	0.097 0.458 0.096	0.022 0.442 0.022
7	SeMet [L588M]	P3 50.0-2.87 (2.92-2.87) 0.97911	74.479/ 84.050	100.0 (100.0) 23.8 (2.07)	0.119 (0.935) 0.125 (0.979) 11.4 (11.5)	0.858 1.696 0.593	0.395 0.222 10.052	-h, -k, l h, -h-k, -l -k, -h, -l	0.110 0.414 0.096	0.108 0.426 0.109	0.022 0.397 0.022
8	SeMet [L588M]	P3 50.0-2.20 (2.24-2.20) 0.97943	73.679/ 83.456	99.9 (100.0) 28.5 (1.61)	0.070 (0.899) 0.076 (0.981) 6.3 (6.3)	0.856 1.686 0.598	0.403 0.230 8.786	-h, -k, l h, -h-k, -l -k, -h, -l	0.090 0.456 0.087	0.100 0.478 0.105	0.022 0.478 0.022
9	SeMet [L588M]	P3 50.0-2.52 (2.56-2.52) 0.97943	73.382/ 83.469	100.0 (100.0) 25.1 (1.62)	0.086 (0.863) 0.094 (0.941) 6.2 (6.3)	0.857 1.691 0.598	0.398 0.225 10.242	-h, -k, l h, -h-k, -l -k, -h, -l	0.089 0.454 0.086	0.105 0.467 0.103	0.022 0.459 0.022
10	SeMet [L588M]	P3 10.0-3.05 (3.10-3.05) 0.97944	73.461/ 83.678	100.0 (100.0) 13.1 (1.95)	0.158 (0.889) 0.173 (0.970) 6.2 (6.3)	0.848 1.742 0.613	0.414 0.241 7.728	-h, -k, l h, -h-k, -l -k, -h, -l	0.088 0.441 0.082	0.105 0.460 0.103	0.022 0.478 0.022

TABLE 1 | Experimental data of ski7-D2/3 crystal and twinning test

Data set #	Construct	Space group Resolution range Wavelength	Unit cell parameter a=b/ c	Completeness I/σ(I)	R-symm Rmeas Redundancy	Wilson ratio <F>^{2}/<F^2> I^2/<I>^{2} <|E^2-1|>	L-test Mean |L| Mean L^2 Z-score	Twin law test			
								Twin operator	Britton analysis	H-test	Maximum likelihood method
11	SeMet [L650M/ I655M]	P3 50.0-3.20 (3.26-3.20) 0.97930	70.944/ 87.043	99.8 (98.5) 15.4 (1.5)	0.129 (0.660) 0.143(0.742) 5.5 (4.6)	0.784 2.098 0.748	0.494 0.324 1.552	-h, -k, l h, -h-k, -l -k, -h, -l	0.017 0.432 0.016	0.035 0.449 0.035	0.022 0.478 0.022
12	SeMet [L650M/ I655M]	P3 50.0-3.40 (3.46-3.40) 0.97960	71.223/ 87.327	100.0 (100.0) 15.8 (2.46)	0.161(0.846) 0.178(0.930) 5.5 (5.8)	0.797 2.023 0.722	0.483 0.313 0.259	-h, -k, l h, -h-k, -l -k, -h, -l	0.022 0.423 0.021	0.044 0.438 0.043	0.022 0.478 0.022
13	SeMet [L650M/ I655M]	P3 50.0-3.00 (3.05-3.00) 0.97930	71.724/ 86.736	98.1 (88.6) 11.8 (1.03)	0.157 (0.866) 0.174 (0.976) 5.4 (4.2)	0.778 2.230 0.758	0.483 0.313 0.259	-h, -k, l h, -h-k, -l -k, -h, -l	0.019 0.427 0.019	0.043 0.450 0.043	0.022 0.478 0.022
14	SeMet [L650M/ I655M]	P3 50.0-3.15 (3.20-3.15) 0.97854	72.559/ 84.450	98.7 (100.0) 23.2 (1.59)	0.096 (0.822) 0.107 (0.904) 5.6 (5.8)	0.779 2.105 0.743	0.505 0.341 1.879	-h, -k, l h, -h-k, -l -k, -h, -l	0.010 0.443 0.010	0.038 0.460 0.035	0.022 0.478 0.022
15	SeMet [L650M/ I655M]	P3 50.0-3.55 (3.61-3.55) 0.97902	72.426/ 85.394	98.8 (100.0) 22.1 (1.91)	0.097 (0.698) 0.109 (0.769) 5.4 (5.6)	0.776 2.175 0.762	0.495 0.327 1.056	-h, -k, l h, -h-k, -l -k, -h, -l	0.025 0.417 0.025	0.059 0.428 0.058	0.022 0.463 0.022
16	SeMet [L650M/ I655M]	P3 50.0-3.10 (3.15-3.10) 0.97884	71.457/ 86.536	99.8 (100.0) 27.0 (2.37)	0.118 (0.946) 0.125 (0.991) 10.6 (11.2)	0.753 2.239 0.805	0.517 0.352 2.747	-h, -k, l h, -h-k, -l -k, -h, -l	0.000 0.444 0.000	0.035 0.467 0.036	0.022 0.457 0.022

[a]Values in parentheses are for reflections in the highest resolution bin.

is a perfect twin, the most difficult case for phasing. During our struggle to overcome this severe problem, the crystal structure of the C-terminal region of Ski7 was reported (Kowalinski et al., 2015) and the atomic coordinates became available (PDB ID: 4ZKD). The molecular replacement trials were successful using the space group $P3_121$, which was initially assigned, however there is a problem in the refinement. In order to determine the correct space group, we examined the self-rotation function of the data processed in lower space group $P3_1$ (Figure 3a). This showed clear three-fold symmetry along *c* axis and interestingly, pseudo two-fold symmetry in one of the axes in the *ab* plane. Therefore, the true space group must be lower symmetry $P3_1$ and the trial gave a clear MR solution using the normal procedure (McCoy, 2007) and there are two molecules in the asymmetric unit (Figure 3b).

Structure of Ski7-D2/3

The crystal structure of Ski7-D2/3 was refined at 2.0 Å resolution with R_{work}/R_{free} factors of 22.5/27.0%, respectively. For a molecular replacement solution, the original data set was used, but for refinement, a twin operator was applied. The twin operator [h,-h-k,-l] gave nearly 10% lower the R_{work}/R_{free} factors, but the other two possible twin operators, [-h,-k,l] and [-k,-h,-l] affected R-factors only marginally. The crystallographic statistics and refinement are given in Table 2. The overall structure of Ski7-D2/3 shows two independent β-barrel structure for each domain 2 and 3 (Figure 4a) and the electron density maps for the core region are excellent (Figure 4b). Domain 2 and 3 are packed tightly and the buried surface area by the contact between two domains is 1,825.4 $Å^2$ out of total 14,600 $Å^2$ surface area of Ski7-D2/3 calculated by PISA server (http://www.ebi.ac.uk/pdbe/prot_int/pistart.html)(Krissinel & Henrick, 2007). A flexible linker region (residues 638-644; region 4) is not visible in the electron density map, but one more residue, Asn637 was built, compared to the molecular replacement template, 4ZKD domain 2 and 3 (Kowalinski et al., 2015). The asymmetric unit contains two monomers, chain A and B, and the root-mean-square deviation (RMSD) between these is 0.814 Å for 213 Cα atom pairs (Figure 5). There are structurally deviated regions (regions 1, 2, 3, and 4) between our Ski7-D2/3 model and the longer model containing GTPase domain (Figure 5).

The structure of Ski7-D2/3 is similar to that of domain 2 and 3 in the other ribosome-associated GTP_{ases}. The Z-scores as determined by the DALI server for Ski7-D2/3 are 15.8, 18.3, 17.2, and 17.3 for free elongation factor 1 alpha-like protein Hbs1 from *Saccharomyces cerevisiae* (PDB ID: 3P26)(van den Elzen et al., 2010), Dom34 complexed Hbs1 from *Schizosaccharomyces pombe* (PDB ID: 3MCA)(Chen, Muhlrad, et al., 2010), archaeal initiation factor 2 gamma subunit from *Sulfolobus solfataricus* (PDB ID: 2AHO)(Yatime *et al*., 2006), and eukaryotic release factor from *Schizosaccharomyces pombe* (PDB ID: 3E20)(Cheng et al., 2009), respectively. As noted, the Ski7-D2/3 shares very limited sequence identity with the corresponding domain of ribosome-associated GTP_{ases} (lower than 20% sequence identity allowing many sequence gaps). When approximately 180 matching Cα atoms of Ski7-D2/3 were superposed with equivalent atoms of the above proteins, the RMSD was in the range of 2.0~2.6 Å. However, the folding pattern and domain orientation was highly conserved (Figure 6).

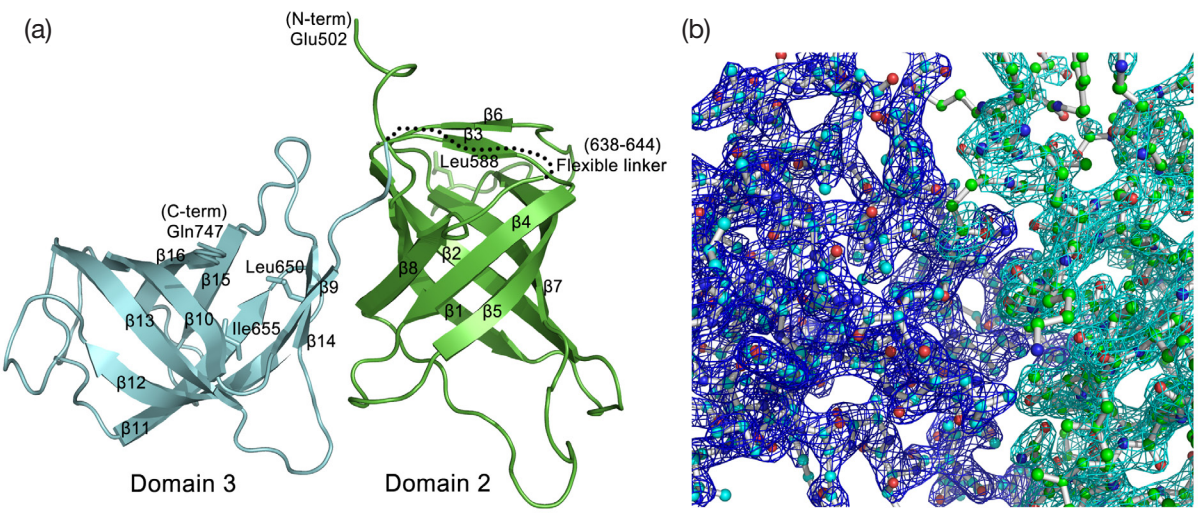

FIGURE 4 | Structure of Ski7-D2/3 and representative electron density map. (a) Overall structure of domain 2 and 3 of Ski7 from *Saccharomyces cerevisiae.* Domains 2 and 3 are colored in green and cyan, respectively. The secondary structural elements of Ski7-D2/3 are indicated. Invisible residues (from Thr638 to Pro644) are indicated as black dots. N- (Glu520) and C-termini (Gln747) of the construct are also indicated. The mutated residues (Leu588, Leu650, and Ile655) are shown as a stick model. (b) The final $2F_o–F_c$ electron density map around the boundary between domain 2 and 3. Cyan and blue colored electron density map correspond to domain 2 and 3, respectively. The map was calculated using 50.0–2.0 Å data and contoured at 1.5 σ.

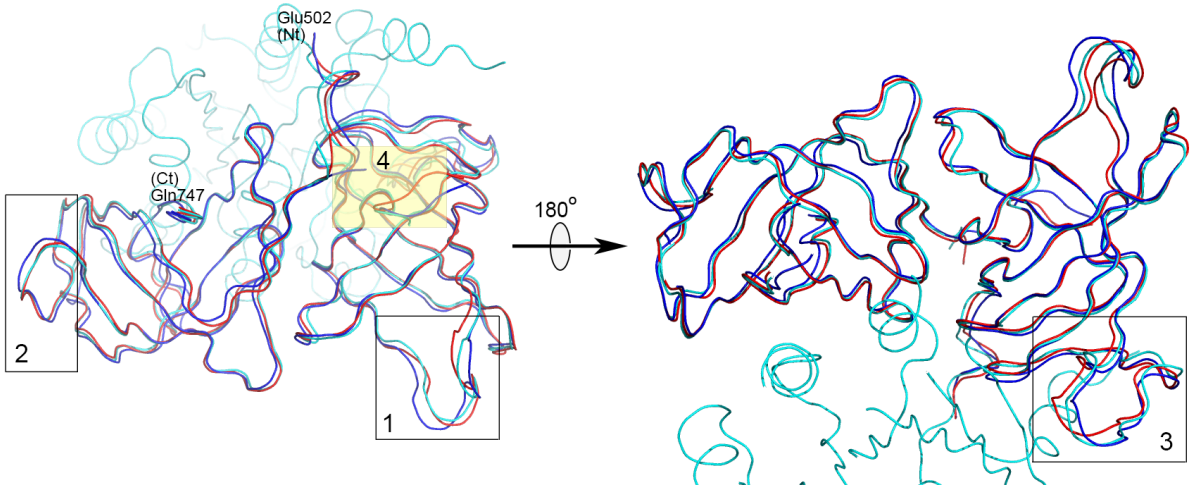

FIGURE 5 | Structural differences among Ski7-D2/3 models. The superposition of Cα traces of two chains (A-chain, blue; B-chain, red) in the asymmetric unit of our Ski7-D2/3 crystal and the molecular replacement template (cyan; PDB ID: 4ZKD). The boxed regions numbered (1, 2, 3, and 4) are structurally the most variant regions. The region 1 (residues 612– 622) locates between β7 and β8 in domain 2, and the region 2 (residues 693–700) between β12 and β13 in domain 3. Region 3 (residues 582–595) in domain 2 contacts with G domain of Ski7. Region 4 shaded with transparent yellow is the flexible linker (residues 638-644), which is invisible in the electron density map. The view left is the same as in Figure 4a and the 180° rotation gives the view right.

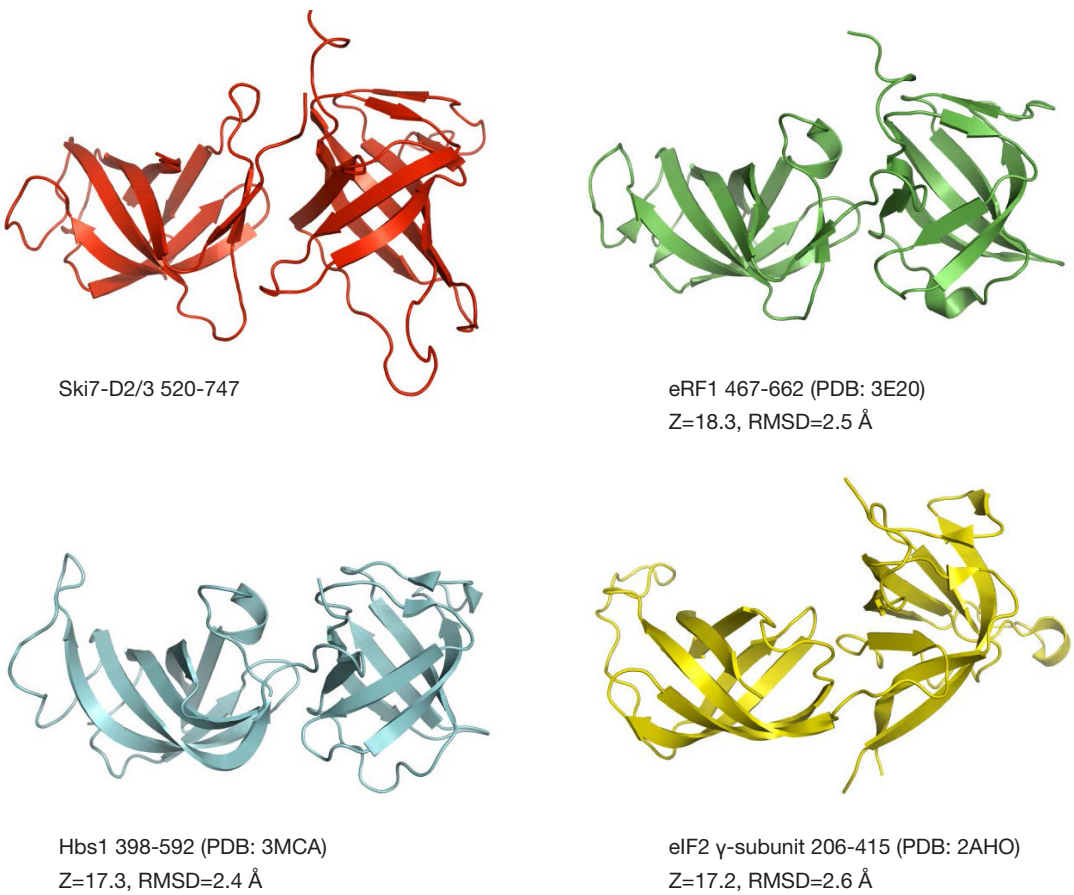

FIGURE 6 | Ribbon diagram comparing the domain 2 and 3 structures of Ski7 (red; top left), eRF1 (green; top right), Hbs1 (cyan; bottom left), and eIF2 (yellow; bottom right). The view is the same as in Figure 4a. PDB ID codes, and Z-scores and root-mean-square deviations (RMSD) from DALI server for each structure are provided.

CONCLUSION

The Ski7-D2/3 crystal has a severe hemihedral twinning problem. Initially, we introduced methionine mutations for better phasing by location of selenium positions, as well as overcoming the twinning problem, because some indicators showed somewhat promising statistics (Table 1). Specifically, Wilson ratio and L-tests of the SeMet data using L650M/I655M double mutant crystals reduced the twin problem, but the twin law test considering three possible twin operators [-h, -k, l], [h, -h-k, -l], and [-k,-h,-l] for trigonal space group clearly shows that the twin fraction α dramatically reduces with the twin operators [-h, -k, l] and [-k,-h,-l], but remains the same with the twin operator [h, -h-k, -l]. The values are nearly 0.5 in all three analyses (Britton analysis, H-test, and Maximum likelihood method), suggesting that the crystal still has the difficult perfect twinning problem. Therefore, we conclude the twin law test with twin operators provided by phenix.xtriage in CCP4 package is the best indicator for twinning and the detection of the twin fraction α for each twin operator is also important for later refinement. We successfully obtained the phases by MR techniques and the reasonable refinement statistics by applying the twin operator (Table 2).

The structure of Ski7-D2/3 is quite similar to that of corresponding domain of ribosome-associated GTP_{ases} (Figure 6). Each domain 2 and 3 forms a β-barrel structure and unique connecting loops (Figure 3a). As shown in Figure 5, an exceptionally long connecting loop between β7 and β8 in domain 2 (region 1), is the most structurally deviated region. Especially the connecting linker between domain 2 and 3 is too

TABLE 2 | Crystallographic statistics and refinement

	Ski7-D2/3 Native 520-747	SeMet L588M	SeMET L650M/I655M
Data collection			
X-ray Source	7A, PAL	5C, PAL	BL44XU, SP8
Resolution (Å)	50-2.00 (2.03-2.00)	50.0-2.20 (2.24-2.20)	50.0-3.10 (3.15-3.10)
Wavelength (Å)	0.97933	0.97943	0.97884
Space group	$P3_1$	$P3_1$	$P3_1$
Unit-cell parameters (a=b, c)	73.528, 83.634	73.679, 83.456	71.457, 86.536
Total reflections	217,015	160,847	95,442
Unique reflections	34,188	25,723	8,970
Completeness (%)	99.8 (99.9)[a]	99.9 (100.0)	99.8 (100.0)
I/σ(I)	33.82 (1.0)	23.8 (2.1)	27.0 (2.37)
R_{symm} (%)[b]	5.9 (81.9)	7.0 (89.9)	11.8 (94.6)
R_{meas} (%)[c]	6.5 (89.7)	7.6 (98.1)	12.5 (99.1)
Redundancy	6.3 (6.0)	6.2 (6.3)	10.6 (11.2)
Refinement			
Resolution (Å)	29.8-2.0	34.9-2.20	35.5-3.09
No. of reflections34,162	34,162	25,709	8,826
Refined twin fraction	0.49/0.51	0.50/0.50	0.50/0.50
Refined twin operator	[h, -h-k, -l]	[h, -h-k, -l]	[h, -h-k, -l]
R_{work}[d]/R_{free}[e]	22.35 / 26.73	22.28 / 26.07	32.37 / 37.41
R.m.s.d.			
Bond lengths (Å)	0.014	0.009	0.006
Bond angles (°)	1.902	1.757	1.244
Ramachandran analysis			
Most favored (%)	98.33%	97.62%	97.86%
Additional allowed (%)	1.67%	2.38%	2.14%

[a]Values in parentheses are for reflections in the highest resolution bin. [b]$R_{symm} = \Sigma_h\Sigma_i|I_{(h,i)}-\langle I_{(h)}\rangle|/\Sigma_h\Sigma_i\, I_{(h,i)}$, where $I_{(h,i)}$ is the intensity of the i^{th} measurement of reflection h and $\langle I_{(h)}\rangle$ is the corresponding average value for all i measurements. [c]$R_{meas} = R_{r.i.m.}$ (redundancy-independent merging R-factor) = $\Sigma_h[N/(N-1)]^{1/2}\Sigma_i(|I_{i(h)}-\langle I_{(h)}\rangle|)/\Sigma_h\Sigma_i I_i(h)$. [d]$R_{work} = \Sigma_{hkl}||F_{obs}|-|F_{calc}||/\Sigma_{hkl}|F_{obs}|$, where F_{obs} and F_{calc} denote observed and calculated structure factors, respectively. [e]R_{free} is calculated for the 10% test set of reflections.

flexible and thus the electron density maps around this region are invisible in all three models of Ski7 (region 4). One might expect that the deviations are originated from the molecular contacts with G domain, especially region 3, but the deviations between chain A and B also show quite significant. Therefore, it is concluded that these regions are intrinsically flexible. Even though the connecting link is flexible, the relative orientation between domain 2 and 3 is virtually the same, because there are quite significant inter-domain contacts (Figure 4b). Therefore, we conclude the Ski7-D2/3 does not show major conformational movement upon contacting with G domain (Figure 5).

METHODS

Cloning and mutagenesis

The gene encoding the Ski7-D2/3 (residues 520-747) was amplified using S. *cerevisiae* genomic DNA by PCR with the primers, 5'-CGCGGATCCGAAACAACTTTGGAAGAGCCATTTG-3' (BamHI site as underlined boldface) and 5'-CTGCTGCTCGAGCTAT TACTGGCATGCAATTCTGC-3' (XhoI site as underlined boldface) as before (*Lee et al*., 2014). For phasing, leucine 650 and isoleucine 655 in Ski7-D2/3 were mutated to methionine residues to express more SeMet containing protein because there is only one methionine in Ski7-D2/3. The mutations were introduced into the Ski7-D2/3 by Quik-change site-directed mutagenesis. The sequences of forward and reverse primer are 5'-GAATTTACCCACACTAAAGTTGATGGCCTTGCGTTTAATGAAATTATCAAT-3' and 5'-GTTTGTATTGATAATTTCATTAAACGCAAGGCCATCAACTTTAGTGT GTTTGGTAAATTC-3' (mutated DNA sequence indicated as underlined boldface). All constructs were confirmed by DNA sequencing. However, the yield of SeMet protein was not high enough using previous GST-fusion vector (*Lee et al*., 2014) and thus, we have changed the expression vector as follows: The PCR products were digested with the BamHI and XhoI restriction enzymes and cloned into the pMAL^{TM}-p4X expression vector modified with an N-terminal His_6-tag followed by MBP (maltose binding protein) tag and a TEV (tobacco etch virus) protease cleavage site (ENLTFQ/G). The plasmids were transformed into *E. coli* BL21(DE3) and B834(DE3) competent cells (Novagen)

Protein expression and purification

To prepare SeMet-labeled Ski7-D2/3, the L650M/I655M double mutant protein was expressed in methionine auxotroph *E. coli* strain B834(DE3). Cells were cultured in minimal medium (Na_2HPO_4, KH_2PO_4, and NH_4Cl), all amino acid stock excluding methionine, vitamins (1 µl of niacinamide), 40 µg/ml SeMet (Wako Pure Chemicals), 0.4% (w/v) glucose (Sigma-Aldrich), $MgSO_4$, and 50 µg/ml ampicillin at 37°C until reaching OD_{600nm} 0.8, and then induced with 0.5 mM isopropyl β-D-thiogalactopyranoside (IPTG, Merck) at 18°C for overnight. The cells were harvested by centrifugation at 8,000 × g at 4°C for 20 min, and the cell pellets were resuspended in cooled buffer A (50 mM Tris-HCl pH 8.0, 200 mM NaCl, and 5 mM 2-mercaptoethanol). The resuspended cells were disrupted by ultrasonication. The cell debris containing insoluble material and the soluble fraction containing the Ski7-D2/3 were separated by centrifugation at 27,000 × g at 4°C for 1 h. The protein was loaded onto the column pre-equilibrated with buffer A and eluted using buffer A containing 500 mM imidazole. The TEV protease was added to the elution fraction with a 1:50 molar ratio to cleave His_6-MBP-tag from Ski7-D2/3 protein at 4°C for overnight. The TEV treated protein was loaded onto the His-Trap column to eliminate the N-terminal His_6-tagged TEV protease and MBP simultaneously because the target protein was not bound to the His column. The Ski7-D2/3 was then concentrated using a 10.0 kDa cutoff Amicon Ultra centrifugal filter device (Millipore). The concentrated sample was filtered by Spin-X centrifuge tube filter (Costar) with pore size of 0.22 µm. The sample was further purified by using a HiLoad 16/60 Superdex 75 pg (GE Healthcare), pre-equilibrated by gel filtration buffer (50 mM Tris-HCl pH 8.0,. 150 mM NaCl, and 1 mM TCEP). After gel filtration chromatography, the protein was purified with high-resolution anion exchange column Mono Q^{TM} (GE healthcare). Fractions containing Ski7-D2/3 were confirmed by 12% (w/v) SDS-PAGE stained with Coomassie Brilliant Blue.

Crystallization

The purified Ski7-D2/3 was concentrated to 7 mg/ml for crystallization. Initial crystals were obtained at the reservoir conditions of 100 mM HEPES-NaOH pH 7.5, 8% (v/v) ethylene glycol, and 10% (w/v) PEG8000 (Wizard Classic 3 tube #12, Rigaku) by hanging-drop vapor diffusion method on 48-well VDX plates at 20°C. The 2 µl drop of 1:1 mixture between Ski7-D2/3 protein and reservoir solution was equilibrated against 140 µl reservoir solution. The crystals were small and grown within the precipitation. An additive screen was performed with Hampton Research additive screen kits. For better crystals, the crystallization drop was mixed in a ratio of 6:3:1 (v/v) for protein solution: reservoir solution: additive solution. In total, 11 additives (2 mM magnesium chloride dehydrate, 2 mM strontium chloride hexahydrate, 10 mM sodium fluoride, 0.6% (v/v) 2-methyl-2,4-pentamediol, 0.6% (v/v) dimethyl sulfoxide, 0.6% (w/v) 6-aminohexaanoic acid, 6 mM glycyl-glycyl-glycine, 3% (v/v) 2-propanol, 0.1% (w/v) polyvinylpyrrolidone K15, 8% (v/v) pentaerythritol ethoxylate, and 0.6% (w/v) D-(+)-galactose) enlarged the crystal size. Although the additives improved the diffraction quality of Ski7-D2/3 crystal, the twinning problem remained the same. The crystallization of SeMet labeled protein was performed in the same way.

Data collection and processing

X-ray diffraction data of the Ski7-D2/3 and its mutants were collected at the beamline 5C and 7A, PAL (Pohang Accelerator Laboratory, Pohang, Korea), the beamline NE3, PF-AR (Photon Factory, Tsukuba, Japan), and the beamline BL44XU, SPring-8 (SPring-8, Hyogo, Japan). Data were recorded using ADSC Quantum 315 CCD detector, processed and integrated using DENZO, and scaled using SCALEPACK from the HKL-2000 program suite (Otwinowski & Minor, 1997). The PHENIX xtriage result for native data showed that the crystal is twinned. Twinning validation was calculated by PHENIX (Adams et al., 2010) and CCP4 program suite (Winn et al., 2011). X-ray data and twinning validation of all data are listed in Table 1.

Structure solution and refinement

The native Ski7-D2/3 and mutants structures were solved by molecular replacement method with PHASER (McCoy, 2007) using corresponding domain of recently reported C-terminal region of Ski7 (PDB ID: 4ZKD) as a search model (Kowalinski et al., 2015). The molecular replacement solution resulted in two D2/3 molecules per asymmetric unit with the space group $P3_1$. The initial model was refined using COOT (Emsley et al., 2010) and PHENIX (Adams et al., 2010). The rigid body refinement and reference model restraints were performed in initial steps of refinement and then non-crystallographic symmetry restraints were applied. Appropriate twin laws [h,-h-k,-l] were applied in final steps of refinement. The assessment of model geometry and assignment of secondary structural elements were achieved using the MolProbity program (Chen, Arendall, et al., 2010). Data collection and refinement statistics are described in Table 2. The DALI server was used for structural comparisons (Holm & Rosenstrom, 2010). All figures for structures were generated using PyMOL (http://www.pymol.org).

ACKNOWLEDGEMENTS

We are grateful to the beamline staff at the 5C beamline of the Pohang

Accelerator Laboratory, Korea and the NW12 beamline of the Photon Factory, Japan for their help during data collection. This study was supported by National Research Foundation of Korea (NRF) grants funded by the Korean government (NRF-2016R1E1A1A01942623 and BRL grant: No. 2015041919) and by a grant from the Institute for Basic Science (IBS-R023-D1). This research was also supported by a Korea University Future Research Grant.

AUTHOR INFORMATION

The authors declare no potential conflicts of interest.

Original Submission: Aug 15, 2015
Revised Version Received: Jan 10, 2017
Accepted: Jan 13, 2017

REFERENCES

Adams, P.D., Afonine, P.V., Bunkóczi, G., Chen, V.B., Davis, I.W., Echols, N., Headd, J.J., Hung, L.W., Kapral, G.J., Grosse-Kunstleve, R.W., McCoy, A.J., Moriarty, N.W., Oeffner, R., Read, R.J., Richardson, D.C., et al. (2010). PHENIX: a comprehensive Python-based system for macromolecular structure solution. *Acta Crystallogr D Biol Crystallogr* **66**, 213-221.

Atkinson, G.C. (2015). The evolutionary and functional diversity of classical and lesser-known cytoplasmic and organellar translational GTPases across the tree of life. *BMC Genomics* **16**, 78.

Breyer, W.A., Kingston, R.L., Anderson, B.F., and Baker, E.N. (1999). On the molecular-replacement problem in the presence of merohedral twinning: structure of the N-terminal half-molecule of human lactoferrin. *Acta Crystallogr D Biol Crystallogr* **55**, 129-138.

Chandra, N., Brew, K., and Acharya, K.R. (1998). Structural evidence for the presence of a secondary calcium binding site in human alpha-lactalbumin. *Biochemistry* **37**, 4767-4772.

Chen, L., Muhlrad, D., Hauryliuk, V., Cheng, Z., Lim, M.K., Shyp, V., Parker, R., and Song, H. (2010a). Structure of the Dom34-Hbs1 complex and implications for no-go decay. *Nat Struct Mol Biol* **17**, 1233-1240.

Chen, V.B., Arendall, W.B., 3rd, Headd, J.J., Keedy, D.A., Immormino, R.M., Kapral, G.J., Murray, L.W., Richardson, J.S., and Richardson, D.C. (2010b). MolProbity: all-atom structure validation for macromolecular crystallography. *Acta Crystallogr D Biol Crystallogr* **66**, 12-21.

Cheng, Z., Saito, K., Pisarev, A.V., Wada, M., Pisareva, V.P., Pestova, T.V., Gajda, M., Round, A., Kong, C., Lim, M., et al. (2009). Structural insights into eRF3 and stop codon recognition by eRF1. *Genes Dev* **23**, 1106-1118.

Dauter, Z. (2003). Twinned crystals and anomalous phasing. *Acta Crystallogr D Biol Crystallogr* **59**, 2004-2016.

Daviter, T., Wieden, H.J., and Rodnina, M.V. (2003). Essential role of histidine 84 in elongation factor Tu for the chemical step of GTP hydrolysis on the ribosome. *J Mol Biol* **332**, 689-699.

Doma, M.K., and Parker, R. (2007). RNA quality control in eukaryotes. *Cell* **131**, 660-668.

Emsley, P., Lohkamp, B., Scott, W.G., and Cowtan, K. (2010). Features and development of Coot. *Acta Crystallogr D Biol Crystallogr* **66**, 486-501.

Frischmeyer, P.A., van Hoof, A., O'Donnell, K., Guerrerio, A.L., Parker, R., and Dietz, H.C. (2002). An mRNA surveillance mechanism that eliminates transcripts lacking termination codons. *Science* **295**, 2258-2261.

Garneau, N.L., Wilusz, J., and Wilusz, C.J. (2007). The highways and byways of mRNA decay. *Nat Rev Mol Cell Biol* **8**, 113-126.

Gill, H.S., Dutcher, L., Boron, W.F., Patel, S., and Guay-Woodford, L.M. (2013). X-ray diffraction studies on merohedrally twinned Delta1-62NtNBCe1-A crystals of the sodium/bicarbonate cotransporter. *Acta Crystallogr Sect F Struct Biol Cryst Commun* **69**, 796-799.

Guelker, M., Stagg, L., Wittung-Stafshede, P., and Shamoo, Y. (2009). Pseudosymmetry, high copy number and twinning complicate the structure determination of Desulfovibrio desulfuricans (ATCC 29577) flavodoxin. *Acta Crystallogr D Biol Crystallogr* **65**, 523-534.

Gutmann, S., Haebel, P.W., Metzinger, L., Sutter, M., Felden, B., and Ban, N. (2003). Crystal structure of the transfer-RNA domain of transfer-messenger RNA in complex with SmpB. *Nature* **424**, 699-703.

Halbach, F., Reichelt, P., Rode, M., and Conti, E. (2013). The yeast ski complex: crystal structure and RNA channeling to the exosome complex. *Cell* **154**, 814-826.

Holm, L., and Rosenstrom, P. (2010). Dali server: conservation mapping in 3D. *Nucleic Acids Res* **38**, W545-549.

Igarashi, N., Moriyama, H., Fujiwara, T., Fukumori, Y., and Tanaka, N. (1997). The 2.8 A structure of hydroxylamine oxidoreductase from a nitrifying chemoautotrophic bacterium, Nitrosomonas europaea. *Nat Struct Biol* **4**, 276-284.

Inada, T. (2013). Quality control systems for aberrant mRNAs induced by aberrant translation elongation and termination. *Biochim Biophys Acta* **1829**, 634-642.

Karzai, A.W., Roche, E.D., and Sauer, R.T. (2000). The SsrA-SmpB system for protein tagging, directed degradation and ribosome rescue. *Nat Struct Biol* **7**, 449-455.

Kong, C., Ito, K., Walsh, M.A., Wada, M., Liu, Y., Kumar, S., Barford, D., Nakamura, Y., and Song, H. (2004). Crystal Structure and Functional Analysis of the Eukaryotic Class II Release Factor eRF3 from *S. pombe*. *Mol Cell* **14**, 233-245.

Kowalinski, E., Schuller, A., Green, R., and Conti, E. (2015). Saccharomyces cerevisiae Ski7 Is a GTP-Binding Protein Adopting the Characteristic Conformation of Active Translational GTPases. *Structure* **23**, 1336-1343.

Krissinel, E., and Henrick, K. (2007). Inference of macromolecular assemblies from crystalline state. *J Mol Biol* **372**, 774-797.

Lee, B.G., Kim, M.K., Kim, B.W., Suh, S.W., and Song, H.K. (2012). Structures of the ribosome-inactivating protein from barley seeds reveal a unique activation mechanism. *Acta Crystallogr D Biol Crystallogr* **68**, 1488-1500.

Lee, H.H., Kim, Y.S., Kim, K.H., Heo, I., Kim, S.K., Kim, O., Kim, H.K., Yoon, J.Y., Kim, H.S., Kim, D.J., Lee, S.J., Yoon, H.J., Kim, S.J., Lee, B.G., Song, H.K., et al. (2007). Structural and functional insights into Dom34, a key component of no-go mRNA decay. *Mol Cell* **27**, 938-950.

Lee, J.Y., Park, S.H., Jeong, B.C., and Song, H.K. (2014). Crystallization and preliminary X-ray analysis of the C-terminal fragment of Ski7 from *Saccharomyces cerevisiae*. *Acta Crystallogr F Struct Biol Commun* **70**, 1252-1255.

Luecke, H., Richter, H.T., and Lanyi, J.K. (1998). Proton transfer pathways in bacteriorhodopsin at 2.3 angstrom resolution. *Science* **280**, 1934-1937.

Lykke-Andersen, J., and Bennett, E.J. (2014). Protecting the proteome: Eukaryotic cotranslational quality control pathways. *J Cell Biol* **204**, 467-476.

Matsuda, R., Ikeuchi, K., Nomura, S., and Inada, T. (2014). Protein quality control systems associated with no-go and nonstop mRNA surveillance in yeast. *Genes Cells* **19**, 1-12.

McCoy, A.J. (2007). Solving structures of protein complexes by molecular replacement with Phaser. *Acta Crystallogr D Biol Crystallogr* **63**, 32-41.

Otwinowski, Z., and Minor, W. (1997). Processing of X-ray diffraction data collected in oscillation mode. *Method Enzymol* **276**, 307-326.

Padilla, J.E., and Yeates, T.O. (2003). A statistic for local intensity differences: robustness to anisotropy and pseudo-centering and utility for detecting twinning. *Acta Crystallogr D Biol Crystallogr* **59**, 1124-1130.

Redinbo, M.R., and Yeates, T.O. (1993). Structure determination of plastocyanin from a specimen with a hemihedral twinning fraction of one-half. *Acta Crystallogr D Biol Crystallogr* **49**, 375-380.

Saito, S., Hosoda, N., and Hoshino, S. (2013). The Hbs1-Dom34 protein complex functions in non-stop mRNA decay in mammalian cells. *J Biol Chem* **288**, 17832-17843.

Schaeffer, D., Tsanova, B., Barbas, A., Reis, F.P., Dastidar, E.G., Sanchez-Rotunno, M., Arraiano, C.M., and van Hoof, A. (2009). The exosome contains domains with specific endoribonuclease, exoribonuclease and

cytoplasmic mRNA decay activities. *Nat Struct Mol Biol* **16**, 56-62.

Shoemaker, C.J., Eyler, D.E., and Green, R. (2010). Dom34:Hbs1 promotes subunit dissociation and peptidyl-tRNA drop-off to initiate no-go decay. *Science* **330**, 369-372.

Shoemaker, C.J., and Green, R. (2012). Translation drives mRNA quality control. *Nat Struct Mol Biol* **19**, 594-601.

Tsuboi, T., Kuroha, K., Kudo, K., Makino, S., Inoue, E., Kashima, I., and Inada, T. (2012). Dom34:hbs1 plays a general role in quality-control systems by dissociation of a stalled ribosome at the 3' end of aberrant mRNA. *Mol Cell* **46**, 518-529.

van den Elzen, A.M., Henri, J., Lazar, N., Gas, M.E., Durand, D., Lacroute, F., Nicaise, M., van Tilbeurgh, H., Seraphin, B., and Graille, M. (2010). Dissection of Dom34-Hbs1 reveals independent functions in two RNA quality control pathways. *Nat Struct Mol Biol* **17**, 1446-1452.

van Hoof, A., Frischmeyer, P.A., Dietz, H.C., and Parker, R. (2002). Exosome-mediated recognition and degradation of mRNAs lacking a termination codon. *Science* **295**, 2262-2264.

Winn, M.D., Ballard, C.C., Cowtan, K.D., Dodson, E.J., Emsley, P., Evans, P.R., Keegan, R.M., Krissinel, E.B., Leslie, A.G., McCoy, A., McNicholas, S.J., Murshudov, G.N., Pannu, N.S., Potterton, E.A., Powell, H.R., et al. (2011). Overview of the CCP4 suite and current developments. *Acta Crystallogr D Biol Crystallogr* **67**, 235-242.

Yatime, L., Mechulam, Y., Blanquet, S., and Schmitt, E. (2006). Structural switch of the gamma subunit in an archaeal aIF2 alpha gamma heterodimer. *Structure* **14**, 119-128.

Yeates, T.O., and Fam, B.C. (1999). Protein crystals and their evil twins. *Structure* **7**, R25-29.

